10.1515/astro-2017-0174

Baltic Astronomy, vol. 23, 93–102, 2014

A DISTANT CHANDRA GALAXY CLUSTER CL J1415.1+3612: CONSTRAINT ON EVIDENCE OF THE COOL-CORE PHENOMENON

Iu. Babyk[1,2,3]

[1] *Main Astronomical Observatory NAS of Ukraine, Zabolotnogo str., 27, 03650, Kyiv, Ukraine*

[2] *Dublin Institute for Advanced Studies, 31 Fitzwilliam Place, Dublin 2, Ireland*

[3] *Dublin City University, Dublin 9, Ireland*

Received: 2014 April 25; revised: May 22; accepted June 8

Abstract. Deep *Chandra* observations of the distant cluster of galaxies, CL J1415.1+3612, are analyzed in order to determine the main physical characteristics of the intracluster medium. We also investigate some properties of a cool-core phenomenon at $\sim$10 kpc. Combining all *Chandra* observations, we derive the average temperature (kT = 6.77$\pm$0.54 keV) and the metal abundance (Z = 0.84$\pm$0.16 $Z_{\odot}$) of the cluster. Assuming hydrostatic equilibrium and spherical symmetry, and using deprojected temperature and surface profiles, we estimate the value of total mass of the cluster within R_{2500}, R_{500} and R_{200} and find the fraction of gas for these radii. The gas mass fraction of CL J1415.1+3612 at R_{500} is typical for X-ray clusters, (2.2$\pm$0.5)$\cdot 10^{14}$ $M_{\odot}$. The total mass is equal to 3.8$\pm$0.4$\cdot 10^{14}$ $M_{\odot}$ at R_{200} and the corresponding gas fraction is f = 0.21$\pm$0.06. In addition, we measured the cooling time of the central region ($\sim$10 kpc) as $t_{\rm cool}$ = 0.163$\pm$0.021 Gyr. The value of entropy in the same region is $K_{\rm c}$ = 12.1$\pm$2.6 keV cm^2. We also checked the redshift value of the cluster using the iron line $K\alpha$ in the X-ray spectra of CL J1415.1+3612. Our analysis makes this galaxy cluster to be one of the best investigated distant massive clusters in the X-ray range.

Key words: galaxies: clusters: intergalactic medium; individual: CLJ1415.1+3612 – X-ray: galaxies: clusters

1. INTRODUCTION

According to the ΛCDM paradigm, the Universe is composed of dark matter, dark energy and baryonic matter (Del Popolo 2007, 2013, 2014, Del Popolo, Pace & Lima 2013a,b). The clusters of galaxies increase their masses as a result of merging between small clusters and groups of galaxies (Del Popolo 2000). Such a model allows to conclude that at high redshifts the clusters should be less massive in comparison with the clusters at small redshifts. Using the modern theoretical approaches and numerical methods of simulations, it is possible to find the total mass profile of the clusters for a given cosmological parameter. As a result, the

comparison of the mass profiles at low and high redshifts is a significant tool for constraining different cosmological parameters.

Galaxy clusters consist of invisible dark matter, hot intracluster medium (ICM) of gas and galaxies. The dominant baryonic component of clusters is the ICM, which is characterized by hot diffuse plasma emitting X-rays via thermal bremsstrahlung. The surface brightness profile of the intracluster medium shows significant peaks in their central areas[1]. The cool cores are observed in almost all bands of the electromagnetic spectrum: ICM in X-rays, cold molecular gas in the infrared, central active galaxy nuclei (AGN) in radio and the brightest cluster galaxies (BCG) in the optical range. It is well known that nuclear activity in the BCG plays an important role in the regulation of different processes inside the cool core, such as thermodynamics of interaction between the ICM and the radio jets (Birzan et al. 2008).

Studies of cool cores of the clusters at high redshifts can provide significant clues on the processes inside the cores, such as the metal enrichment. The two major X-ray telescopes, *Chandra* and *XMM-Newton* are still the best instruments to find and characterize distant galaxy clusters.

A few tens of distant clusters are known, which have been confirmed spectroscopically as the objects at high redshifts ($z > 1$). Most of them have been detected in infrared surveys. In this paper, we perform a detailed investigation of X-ray properties of the galaxy cluster CL J1415.1+3612 (hereafter CLJ1415) at $z = 1.03$ using observations from the *Chandra* telescope.

The cluster CLJ1415 was discovered in the Wide Angle Rosat Pointed Survey (hereafter WARPS, Jones et al. 1998). WARPS contains a sample of 129 galaxy clusters down to a flux limit of $\sim 6.5 \times 10^{-14}$ erg s^{-1} cm^2.

The properties of the surface brightness profile show that CLJ1415 can be the strongest high-redshift cool-core cluster (Santos et al. 2010, 2012). It is also one of the deepest clusters observed with *Chandra*. Santos et al. (2012) from the *Chandra* observations have found $kT = 6.82$ keV and $Z = 0.88 Z_\odot$. Using the strong $K\alpha$ iron line, they have also found that the redshift of CLJ1415, with the accuracy ¡ 1%, is $z = 1.028$. They have found the total mass of the cluster, $M_{500} = 2.4 \pm 0.4\, M_\odot$.

The plan of the present paper is the following. In Section 2 we describe the X-ray observations and data analysis of the *Chandra* archive data, which provide the main properties of CLJ1415. In Section 3 we describe the spectral analysis and in Section 4 we give the results of analysis and discussion of the surface brightness and the total mass profiles. Section 5 is devoted to conclusions.

Through the paper we adopt the following cosmological parameters: $H_0 = 73$ km s^{-1} Mpc^{-1} and the matter density $\Omega_\mathrm{m} = 0.27$.

2. THE SOURCE OF X-RAY MEASUREMENTS AND DATA REDUCTION

The list of the archival observations of CLJ1415 with *Chandra* and *XMM-Newton* X-ray telescopes is given in Table 1. The overall exposure time with *Chandra* is ∼370 ks. It is one of the longest exposure among the distant galaxy clusters with $z \simeq 1$.

[1] The cooling time in the cluster centers, the so-called cool-core phenomenon, is shorter than the dynamical time.

Table 1. The list of X-ray observations of CLJ1415.

ID	Time	Instrument	Exposure time
Chandra			
4163	2003-09-16	ACIS-I	90.37
12256	2010-08-28	ACIS-S	120.04
12255	2010-08-30	ACIS-S	61.19
13118	2010-09-01	ACIS-S	45.23
13119	2010–9-05	ACIS-S	55.04
XMM-Newton			
0148620101	2003-08-03	MOS, PN	45.79

Unfortunately, the *XMM-Newton* data have low levels of the useful exposure time (17 ks for MOS and 14 ks for PN). In addition, the instruments of *XMM-Newton* have lower angular resolution. As a result, we do not use these data in our analysis.

For data reduction, we used the CIAO 4.3 software package with the latest calibration database (CalDB 4.5.1). A detailed information about the data reduction has been given in our previous articles (Babyk et al. 2012a,b,c; Babyk & Vavilova 2012, 2013a,b, 2014). The data reduction is performed as follows: all point sources in the images were identified and removed, then images of the cluster were split to concentric annuli. The annulus for background was also created with the same size and without any sources inside.

3. SPECTRAL ANALYSIS

We constructed images of the cluster in the 0.5–7.0 keV energy band. The spectral analysis was made in the following sequence: the X-ray peak on images was found and the concentric rings with about 2000±50 X-ray photons inside the 0.5–7.0 keV energy range were drawn. We formed 10 rings with different radii, and for each of them the spectra were extracted with the *specextract* tool. The response matrix files (*arf*) and the ancillary response files (*rmf*)[2] for each spectrum were extracted by summing over all five *Chandra* observations using the *addarf* and *addrmf* routines, respectively. In the same way, we have created the background spectra (Babyk 2012c).

To analyze the spectra, we used Xspec 12.6.0 code (Arnaud 1996) and a MEKAL model (Kaastra & Mewe 1993; Liedahl et al. 1995) with the parameter WABS, which was taken from Dickey & Lockman (1990) as $N_{\rm H} = 1.22\times 10^{20}$ cm^{-2}. The redshift parameter in the MEKAL model was fixed as $z = 1.03$. All spectra were binned by 30 photons per bin. The parameter of metal abundance was fixed as $Z = 0.3\ Z_{\odot}$. In addition, the average temperature and abundance was obtained in the available region (about 30″) centered around the cluster position. The best fit parameters are $kT = 6.77\pm0.54$ keV and $Z = 0.84\pm0.16\ Z_{\odot}$. The errors are calculated for 68% of the confidence level. These values are in good agreement with the previous measurements by Santos et al. (2012) and Maughan et al. (2006, 2008) for the *XMM-Newton* and *Chandra* ACIS-I analysis.

The observed projected temperature profile is shown in Figure 1. We found

[2] These files are necessary to perform spectral fitting in Xspec.

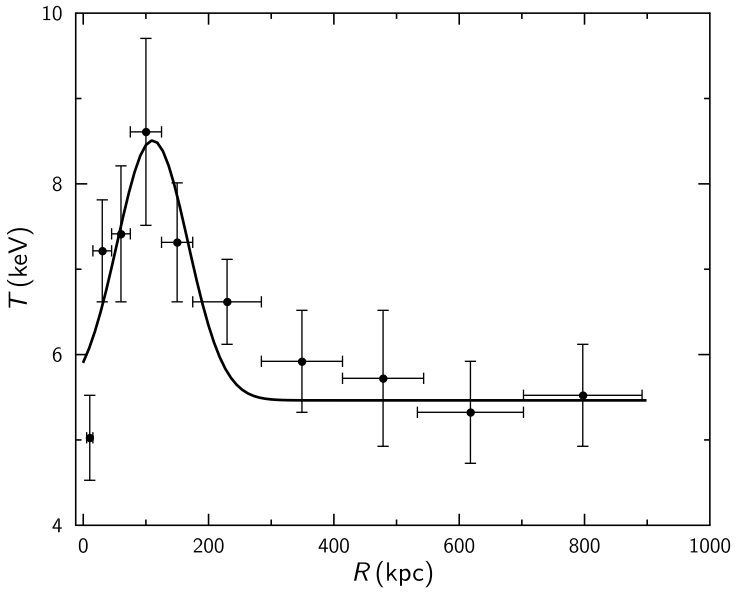

Fig. 1. The observed projected temperature profile of CLJ1415 and the corresponding fit from the DSDEPROJ routine.

the temperature profile out to ~ 1 Mpc with an accuracy of 10% for the 68% confidence level. The inner bin had a size of ~ 5 kpc and was deleted. The previous results showed a drop in temperature from 11.0 ± 2.6 to 6.5 ± 1.7 keV in the core of CLJ1415 (Foley et al. 2011), with a drop factor of 1.7 ± 0.5, and from 22 ± 6 to 6.6 ± 0.7 keV in the core of CL J0102-4215 at $z = 0.87$ (Menanteau et al. 2011), with a drop factor ~ 2. Santos et al. (2012) found a significant central temperature drop with 4.6 ± 0.4 keV at $r < 20$ kpc, and 8.0 ± 1.2 keV at $r = 80$ kpc. It is evident, the temperature decrease in the central part of the cluster is a very sensitive test which depends on the method of measuring the temperature in the cool core. Therefore, we have rejected the central peaks of images to determine the projected temperature profile. The annular spectra were modeled in order to determine the deprojected X-ray temperature, metalicity and entropy profiles. We used the deprojection routine *DSDEPROJ* (Sanders & Fabian 2007); Russell et al. 2008).

The peak in the metal abundance distribution is usually associated with the presence of a cool core in the intracluster medium. Here we show the spatial distribution of metalicity in CLJ1415 out to 800 kpc (Figure 2). An unusual Fe abundance, $Z/Z_{\odot} = 3.8 \pm 1.2$, has been found.

Galaxy clusters can be either with the cool cores or without them. This depends on the value of their cooling time and entropy. Using the deprojected gas density and temperature profiles (see below), we extract the entropy profile shown in Figure 3. We used the quantity $K(r) = kTn_{\rm e}^{-2/3}$ as entropy to describe the thermodynamical behavior of the intracluster medium of CLJ1415. Previous investigations of clusters at low redshift have shown that the clusters with a cool core have lower entropy ($K_{\rm c} < 30$ keV cm^2) than the clusters without cool core (Cavagnolo et al. 2008). We found that the central gas entropy of CLJ1415 in the

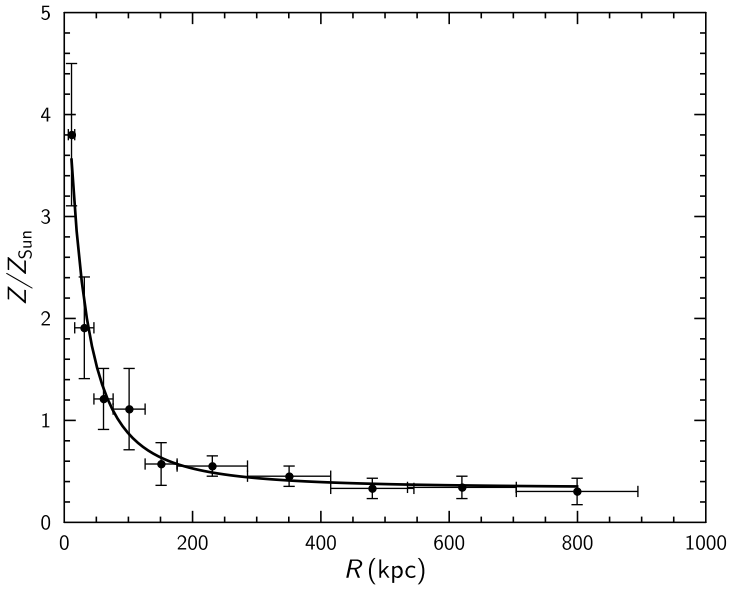

Fig. 2. The observed projected metalicity profile of CLJ1415 in solar units and the corresponding fit from *DSDEPROJ*.

innermost bin (~ 10 kpc) is $K_{\rm c} = 12.1 \pm 2.6$ keV cm^2.

We used an isobaric cooling model for the gas to calculate $t_{\rm cool}$:

$$t_{\rm cool}(r) = \frac{2.5 n_{\rm g} T}{n_{\rm e}^2 \Lambda(T, Z)}, \tag{1}$$

where $\Lambda(T, Z)$ is the cooling function, $n_{\rm g}$ and $n_{\rm e}$ are the gas and electron densities, and T is the temperature. The relation $n_{\rm g} = 1.9\, n_{\rm e}$ was taken from Peterson & Fabian (2006). For the central part of the cluster (~ 10 kpc) we found that $t_{\rm cool} = 0.163 \pm 0.021$ Gyr.

In addition, we checked the value of redshift from X-ray observations using the property of the K_α iron line complex. Note, that we need approximately 1000 counts to calculate $z_{\rm X}$ for a 3σ confidence level. We run a combined fit on the ACIS-S spectra. The values of temperature, metalicity and normalization during the modeling were let free. We found that the best-fit value of redshift is 1.02 ± 0.02. The redshift was estimated from the X-ray observations at $\sim 2.7\sigma$ confidence level. As reported above, in modeling of the annular spectra, we used z=1.03 coinciding with $z_{\rm X}$=1.03.

4. TOTAL MASS PROFILE

4.1. Surface brightness profile

In order to obtain the surface brightness profile, we used the ACIS-S images of the cluster and the *Sherpa* software package of CIAO. The brightness profile was described by a single β-model (Cavaliere & Fusco-Femiano 1978)

$$S(r) = S_0 (1 + (r/r_c)^2)^{-3\beta+0.5} + C. \tag{2}$$

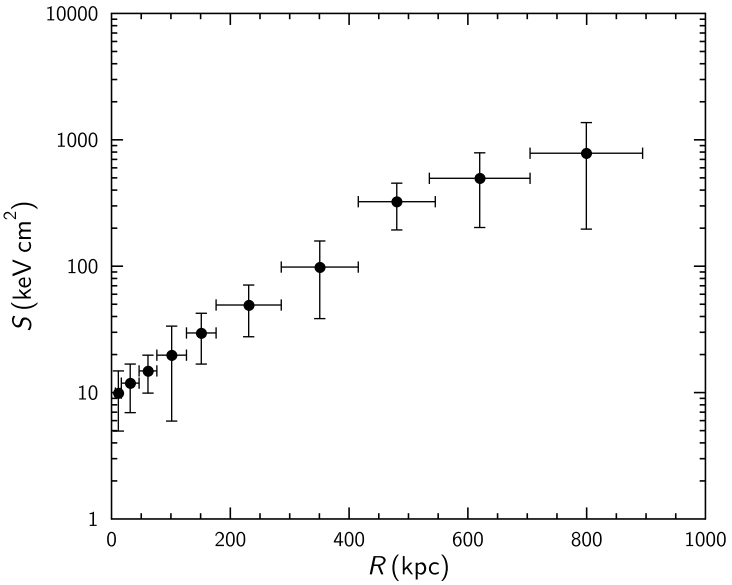

Fig. 3. The observed entropy profile of CLJ1415 obtained from the deprojected temperature and density profiles.

where $S(r)$ is the X-ray surface brightness profile as a function of the projected radius r, S_0, r_c, β and C are free parameters in fitting the model to the X-ray surface brightness profile. In general the X-ray surface brightness profile is well modeled by the β-model (see also Del Popolo 2002; Del Popolo, Hiotelis, Penarrubia 2005).

The best-fit parameters are $\beta = 1.2$ and $r_c = 254$ kpc for $\chi^2 = 0.93/12$ depth of the field (Figure 4). Systematic uncertainties for the profile parameters are small.

Several examples exist when the standard β-model leads to underestimating the brightness in central regions of galaxy clusters. The central X-ray excess is one of the first evidences of cooling flows in clusters (Jones & Forman 1984). For simplicity, in our study we use a single β-model (like in Roncarelli et al. 2006).

We found the well known parameter called surface brightness concentration (c_{SB}) which is significant and useful when we deal with the low S/N data. The measured value of this parameter is $c_{SB} = 0.152 \pm 0.012$ using the combined 370 ks ACIS observations. Santos et al. (2010, 2012) have found c_{SB} as 0.144 ± 0.016 and 0.150 ± 0.007, respectively, that are in agreement with our calculations.

4.2. Mass distribution

The next step of our work is to determine total mass of the cluster and a fraction of gas in the total mass. It is known that baryonic mass can be estimated using the three-dimensional electron density profile. For a single β-model such profile is given as

$$n_e(r) = n_{e0}[(1 + (r/r_c)^2)^{-3\beta/2}]. \quad (3)$$

To compute n_{e0} we used the relation between the electron and proton densities of

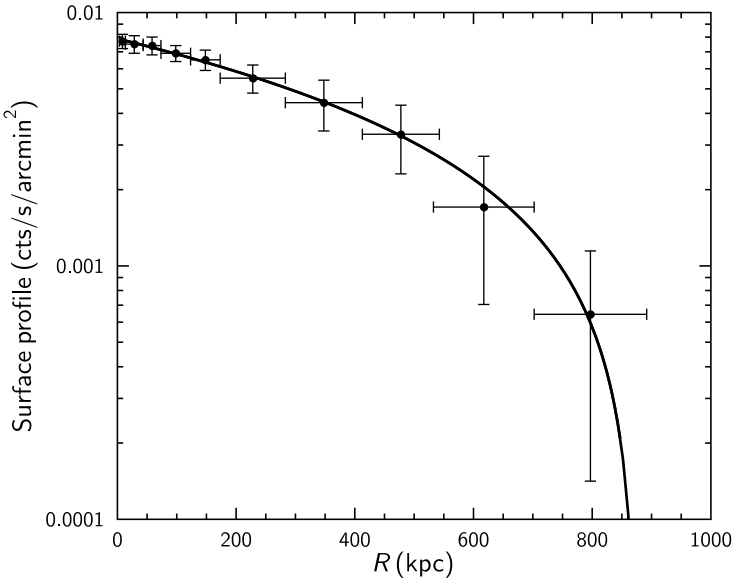

Fig. 4. The surface brightness profile in the energy range 0.5–7.0 keV and the best-fit β-model for CLJ1415.

Table 2. Total mass and gas fraction for the three radii in CLJ1415.

Δ	R_Δ (kpc)	$M_{\rm tot}$ ($M_\odot$)	f_g
2500	318±34	(4.4±0.3)·10^{13}	0.075±0.011
500	652±57	(2.2±0.5)·10^{14}	0.12±0.04
200	938±74	(3.8±0.4)·10^{14}	0.21±0.06

diffuse gas in the MEKAL model and the normalization parameter

$$Norm_{\rm MEKAL} = \frac{10^{14}}{4\pi D_{\rm A}^2 (1+z)^2} \int n_{\rm e} n_{\rm H} dV, \tag{4}$$

where $D_{\rm A}$ is the angular distance to the cluster (in cm), and $n_{\rm e}$ and $n_{\rm H}$ are the electron and hydrogen concentrations, respectively. As the result, we have found that $n_{\rm e0} = (1.02 \pm 0.16) \times 10^{-2}$ cm^{-3}.

To reconstruct the total mass of CLJ1415, we have used the assumptions of hydrostatic equilibrium and spherical symmetry, which leads to the equation

$$M(r) = -4.0 \times 10^{13} M_\odot T({\rm keV}) r({\rm Mpc}) \left(\frac{d\log(n_{\rm e})}{d\log r} + \frac{d\log(T)}{d\log r} \right). \tag{5}$$

We calculated the total mass profile at z=1.03. As a result we can solve the equation $M_\Delta(r_\Delta) = \Delta 4/3\pi r_\Delta^3 \rho_c(z)$ to determine the radius where the average density value is Δ. We found the mass estimates for Δ = 2500, 500 and 200. The results are summarized in Table 2.

The total mass profile is shown in Figure 5 (dotted line) with the corresponding $1\,\sigma$ confidence level. The error intervals are estimated using the assumption that

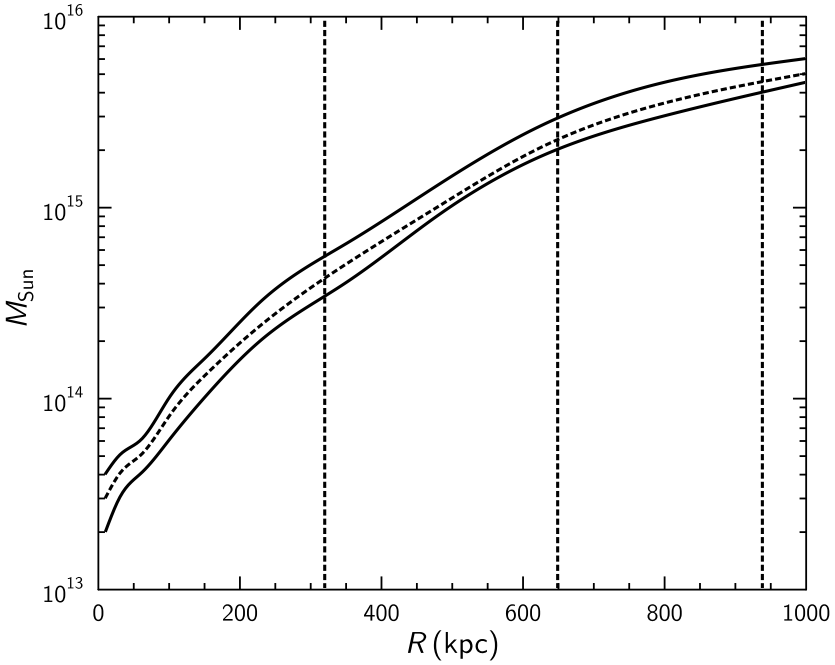

Fig. 5. The total mass profile for CLJ1415 (dotted line). Two solid lines above and below the profile demonstrate $1\,\sigma$ confidence level. The dashed vertical lines show R_{2500}, R_{500} and R_{200}, from left to right.

the relative errors of the deprojected temperature profile are the same as those on the projected values.

Jee et al. (2011) found the total mass $M_{\rm tot}(r < 1.09{\rm Mpc}) = 4.7 \pm 2.0 \times 10^{14} M_{\odot}$ using the weak lensing analysis of WARPS J1415 for the HST/ACS data, that is in agreement with the X-ray mass M_{200}. We also obtained a fraction of baryons in the total mass shown in Table 2. The value at R_{500} is typical for other distant galaxy clusters (Ettori et al. 2009). Muchovej et al. (2007) for CLJ1415 have made measurements of the Sunyaev-Zeldovich effect. They used observations obtained at 30 GHz using eight-element the Sunyaev-Zeldovich Array (SZA) interferometer. They estimated the electron temperature, gas mass and total cluster mass from the Sunyaev-Zeldovich data assuming isothermality and hydrostatic equilibrium for the ICM at a moderate redshift. The total mass was integrated approximately to the virial radius and was found to be $1.9^{+0.5}_{-0.4} \times 10^{14} M_{\odot}$. All the quantities obtained by Muchovej et al. (2006) are in good agreement with the cluster physical characteristics measured from X-ray estimations. They also found the value of total mass at $R_{200} = 0.70 \pm 0.09$ Mpc as $1.86^{+0.45}_{-0.35} \times 10^{14} M_{\odot}$. The fraction of hot gas at this radius was found to be 0.161 ± 0.05. In addition, they estimated the total mass within $R_{2500} = 0.17 \pm 0.04$ Mpc as $3.1 \pm 0.8 \times 10^{13} M_{\odot}$. The authors have concluded that the Sunyaev-Zeldovich temperature (~ 4 keV) is marginally smaller than the value derived from X-rays (~ 6 keV).

Using the *Chandra* data, Santos et al. (2012) got a significant result towards understanding the possible cosmological evolution of the central feedback in clusters of galaxies, and refining Active Galactic Nuclei feedback prescriptions in galaxy

evolution models at high-z.

It is important to note, that a comparison of our results with the cosmological simulations can provide additional new constraints to the cluster formation scenarios, which we plan to verify in our future work.

5. CONCLUSIONS

In this work we have studied a distant galaxy cluster CLJ1415.1+3612 using the results of deep observations with the *Chandra* X-ray Observatory for analysis of the ICM and the cool-core phenomenon. We determined the following physical parameters of CL J1415.1+3612: (a) the temperature is $kT = 6.77 \pm 0.54$, (b) the metal abundance $Z = 0.84 \pm 0.16$ in solar units, (c) the cooling time of the cool core (~ 10 kpc) is $T_{\rm cool} = 0.163 \pm 0.021$ Gyr, and (d) the entropy of the cool core is $K_{\rm c} = 12.1 \pm 2.6$ keV cm^2.

Using the assumptions of hydrostatic equilibrium and spherical symmetry, we constructed the surface brightness, density and total mass profiles, and estimated the mass values for different radii ($R_{2500}, R_{500}, R_{200}$). The total mass of CLJ1415.1+3612 at R_{200} is $M_{\rm tot} = (3.8 \pm 0.4) \cdot 10^{14}\ M_{\odot}$, and the fraction of gas at this radius is equal to 0.21 ± 0.06 % of total mass.

Our investigation shows that CLJ1415.1+3612 has a well-recognized cool core with intracluster medium properties similar to clusters at low redshifts. The presence of a strong metallicity peak near the cluster center is found. This means that the central region has been promptly enriched in metals by star formation processes inside the central galaxy. Our results constrain time-scale for the formation of the cool core of CLJ1415.1+3612.

Additionally, we compared the cluster parameters derived by our X-ray method and the Sunyaev-Zeldovich method. A good agreement between all derived parameters is found, except of a marginally inconsistent value of the temperature. We also discussed the issues which affect the temperature determination in the Sunyaev-Zeldovich and X-ray methods.

ACKNOWLEDGMENTS. This research has made use of data obtained from the *Chandra* Data Archive and Source Catalog, and the software provided by the *Chandra* X-ray Center (CXC). The HEASARC online data archive at NASA/GSFC has been extensively used. This work is partially supported by the Target Program of Space Science Research of the National Academy of Science of Ukraine (2012–2016).

REFERENCES

Arnaud K. 1996, in *Astronomical Data Analysis Software and Systems. V*, ASPC, 101, 17

Babyk Iu., Elyiv A., Melnyk O., Krivodubskij V. N. 2012a, Kinematics and Physics of Celestial Bodies, 28, 69

Babyk Iu., Melnyk O., Elyiv A. 2012b, Advances in Astronomy and Space Physics, 2, 56

Babyk Iu., Vavilova I. 2014, Ap&SS, 349, 415

Babyk Iu. 2012c, Bull. Crimean Astrophys. Obs., 108, 87

Babyk Iu., Melnyk O., Elyiv A. 2012, Advances in Astronomy and Space Physics, 2, 188

Babyk Iu., Vavilova I. 2012, Odessa Astron. Publ., 25, 119
Babyk Iu., Vavilova I. 2013a, Odessa Astron. Publ., 26, 175
Babyk Iu., Vavilova I. 2013b, arXiv:1302.0873
Birzan L., McNamara B. R., Nulsen P. E. J. et al. 2008, ApJ, 686, 859
Cavagnolo K. W., Donahue M., Voit G. M., Sun M. 2008, ApJ, 683, L107
Cavaliere A., Fusco-Femiano R. 1978, A&A, 70, 677
Del Popolo A. 2002, MNRAS, 337, 529
Del Popolo A. 2007, Astron. Rep., 51, 169
Del Popolo A. 2013, AIP Conf. Proc., 1548, 2
Del Popolo A. 2014, Int. J. Mod. Phys. D, 23, 1430005
Del Popolo A., Gambera M. 2000, A&A, 357, 809
Del Popolo A., Pace F., Lima J. 2013a, MNRAS, 430, 628
Del Popolo A., Pace F., Lima J. 2013b, IJMPD, 22, id. 1350038
Del Popolo A., Hiotelis N., Penarrubia J. 2005, ApJ, 628, 76
Dickey J. M., Lockman F. J. 1990, ARA&A, 28, 215
Ettori S., Morandi A., Tozzi P. et al. 2009, A&A, 501, 61
Foley R. J., Andersson K., Bazin G. et al. 2011, ApJ, 731, 86
Jee M. J., Dawson K. S., Hoekstra H. et al. 2011, ApJ, 737, 59
Jones C., Forman W. 1984, ApJ, 276, 38
Jones L. R., Scharf C., Ebeling H. et al. 1998, ApJ, 495, 100
Kaastra J. S., Mewe R. 1993, A&AS, 97, 443
Liedahl D. A., Osterheld A. L., Goldstein W. H. 1995, ApJ, 438, L115
Maughan B. J., Jones L. R., Ebeling H., Scharf C. 2006, MNRAS, 365, 509
Maughan B. J., Jones L. R., Pierre M. et al. 2008, MNRAS, 387, 998
Menanteau F., Hughes J. P., Sifon C. et al. 2012, ApJ, 748, 7
Muchovej S., Mroczkowski T., Carlstrom J. et al. 2007, ApJ, 663, 708
Peterson J. R., Fabian A. C. 2006, Phys. Rep., 427, 1
Roncarelli M., Ettori S., Dolag K. et al. 2006, MNRAS, 373, 1339
Russell H. R., Sanders J. S., Fabian A. C. 2008, MNRAS, 390, 1207
Sanders J. S., Fabian A. C. 2007, MNRAS, 381, 1381
Santos J. S., Tozzi P., Rosati P., Bohringer H. 2010, A&A, 521, A64
Santos J. S., Tozzi P., Rosati P. et al. 2012, A&A, 539, A105